Controllable quantum phase transition in a double-cavity magnonic system

Yan Qin, Sheng-Chang Li,* Ke Li, and Juan-Juan Song

Ministry of Education Key Laboratory for Nonequilibrium Synthesis and Modulation of Condensed Matter, Shaanxi Province Key Laboratory of Quantum Information and Quantum Optoelectronic Devices, School of Physics, Xi'an Jiaotong University, Xi'an 710049, China

(Received 18 May 2022; revised 3 August 2022; accepted 4 August 2022; published 16 August 2022)

We propose a theoretical model to study the quantum phase transition in a double-cavity magnonic system. We find that the system exhibits a second-order phase transition from a parity-symmetric phase to a parity-symmetry-broken phase or a first-order phase transition from a parity-symmetric phase to a bistable phase when the driving strength of one cavity is above a critical value. We obtain the phase diagram, the critical point, and the corresponding critical exponent to characterize the phase transition. We can identify different phase transitions by the different behaviors of the mean magnon number and correlation fluctuation in the vicinity of the critical point. In particular, we show that the phase transition in one cavity can be precisely and efficiently controlled by adjusting the parameters of the other cavity, which suggests that we can easily observe the phase transition at low driving strength in experiment. The effects of additional microwave pulses on the dynamical behavior of the phase-transition observable and the experimental feasibility of our theoretical scheme are discussed as well.

DOI: 10.1103/PhysRevB.106.054419

I. INTRODUCTION

Over the last few decades, the quantum phase transition (QPT) has won extensive concern and has made remarkable achievements in the aspects of theory and application [1–5]. Many research works are mainly carried out from the perspectives of dynamical QPT [6–8], dynamics of QPT [9–11], and steady-state QPT. The steady-state QPT can be divided into ground-state phase transition [12–14] and excited-state phase transition [15,16]. To investigate the QPT, many approaches have been proposed [17–22] including Langevin, pseudospin, extended coherent-state, tensor-entanglement renormalization group, Chern-Simons fermionization, unitary time evolution, and reduced density operator approaches. In addition, many concepts have been adopted to characterize the QPT in quantum information [23–30], such as fidelity, entanglement, quantum Fisher information, entropy, and quantum discord, which make the QPT easier to be observed in experiment and better to be applied in practice. There have already been a plethora of systems to study QPT [31–35]. Research on QPT has made important progress in hybrid cavity magnonic systems in recent years. In Ref. [36], the authors studied the parity-symmetry-breaking QPT in a single-cavity magnonic system which was driven by a parametric field. The parity-symmetric phase (PSP), the parity-symmetry-broken phase (PSBP), and the bistable phase (BP) were obtained in their work.

Recently, considerable efforts have been made in the study of the topics about cavity magnons both theoretically and experimentally [37–42]. The cavity magnonic system attracts much attention because it has many advantages and characteristics. Strong controllability is an important aspect of this system, especially in frequency. There are a great number of novel physical phenomena occurring in the cavity magnonic system, i.e., magnon Kerr effect [43,44], nonreciprocity [45–48], cavity magnon polariton [49–51], and so on. The researchers also show solicitude for the parity-time symmetry [52,53] or anti-parity-time symmetry [54,55] of the cavity magnonic system.

As mentioned previously, the QPT has been demonstrated in a single-cavity magnonic system [36]. However, in this system the phase transition occurs only at special positions, which is inconvenient for experimental observation of the phase transition. To make the research on phase transition in cavity magnonic systems more perfect, in this paper we propose a theoretical model in which an auxiliary cavity is introduced. We mainly study the controllable QPT in a double-cavity magnonic system which contains a main cavity and an auxiliary cavity. There are three phases obtained in our system, namely, PSP, PSBP, and BP. We find that the system experiences a second-order phase transition from a PSP to a PSBP or a first-order phase transition from a PSP to a BP when the driving strength of one cavity is above a critical value. We obtain a lower critical driving strength, which provides a solid theoretical support for easily observing the phase transition in experiment. Furthermore, we investigate the different behaviors of the mean magnon number and correlation fluctuation in the vicinity of the critical point and find that these behaviors can be used to identify different phase transitions.

It should be noted that, when studying the QPT in our double-cavity magnonic system, the roles played by the two cavities are essentially equivalent due to the decoupling between them. However, this paper focuses on the control of phase transition, which requires a distinction between the functions of the two cavities. We use the main cavity to observe the QPT and use the auxiliary cavity to control the QPT.

*scli@xjtu.edu.cn

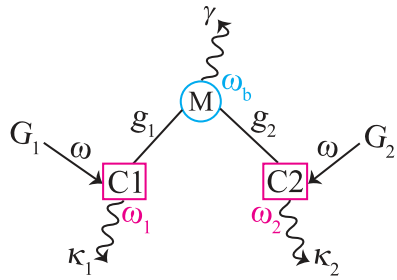

FIG. 1. Schematic of the double-cavity magnonic system, which includes two microwave cavities (C1 and C2) and one yttrium iron garnet sphere (M). $\omega_{1,2}$ and ω_b are the frequencies of the cavity modes and magnon mode, respectively. $\kappa_{1,2}$ is the decay of the cavity modes and γ is the damping of the magnon mode. $G_{1,2}$ refers to the driving amplitude for both cavities with frequency ω. $g_{1,2}$ indicates the coupling between the cavity mode and magnon mode.

We show that the QPT in the main cavity can be precisely and efficiently controlled by adjusting the parameters of the auxiliary cavity, which illustrates the superiority of our system in experimental observation over the single-cavity magnonic system [36]. Moreover, we believe that a different phase may appear in our system when the two cavities interact with each other, which will be studied in the future work. We hope the scheme proposed in this paper can promote further experimental research.

The rest of the paper is organized as follows. In Sec. II, we propose a model to describe a double-cavity magnonic system, present the dynamical equations of expectation values for the cavity mode and magnon mode, and obtain the steady-state solutions for the mean magnon number. In Sec. III, we demonstrate the controllability of QPT. In addition, we use the mean magnon number and the mean correlated fluctuation to characterize the controllable QPT. The discussions and conclusions are presented in Sec. IV.

II. MODEL

We propose a double-cavity magnonic model including two cavity modes and one magnon mode as illustrated in Fig. 1 and the Hamiltonian is ($\hbar = 1$)

$$H = \sum_{j=1,2}\Big[\omega_j a_j^\dagger a_j + g_j(a_j b^\dagger + a_j^\dagger b) + \frac{G_j}{2}(a_j a_j e^{i\omega t} + \text{H.c.})\Big] + \omega_b b^\dagger b + \frac{K}{2} b^\dagger b^\dagger b b, \tag{1}$$

where $a_j^\dagger$ (a_j) is the creation (annihilation) operator for cavity mode j with frequency ω_j. The cavity Cj is driven by a monochromatic field with amplitude G_j and frequency ω. b ($b^\dagger$) is the annihilation (creation) operator of the magnon mode with frequency ω_b. K denotes the Kerr coefficient. g_j indicates the coupling between the magnon mode b and the cavity mode j. For more details about model (1) please see Appendix A.

In a rotating frame with $U = e^{-i\omega(\sum_{j=1,2} a_j^\dagger a_j + b^\dagger b)t/2}$, the Hamiltonian (1) can be rewritten as

$$H = \sum_{j=1,2}\Big[\Delta_j a_j^\dagger a_j + g_j(a_j b^\dagger + a_j^\dagger b) + \frac{G_j}{2}(a_j a_j + \text{H.c.})\Big] + \Delta_b b^\dagger b + \frac{K}{2} b^\dagger b^\dagger b b, \tag{2}$$

where $\Delta_j = \omega_j - \omega/2$ is the frequency detuning between the cavity mode j and the driving field. $\Delta_b = \omega_b - \omega/2$ is the frequency detuning between the magnon mode and the driving field.

By introducing dissipation into the Hamiltonian (2) [56–58], we can give the dynamical equations as follows:

$$\frac{da_j}{dt} = -iP_j a_j - iG_j a_j^\dagger - ig_j b + \sqrt{2\kappa_j}a_j^{\text{in}}, \tag{3}$$

$$\frac{db}{dt} = -iQb - ig_1 a_1 - ig_2 a_2 - iKb^\dagger b b + \sqrt{2\gamma}b^{\text{in}}, \tag{4}$$

where $P_j = \Delta_j - i\kappa_j$ and $Q = \Delta_b - i\gamma$ with κ_j being the decay of cavity mode j and γ being the damping of magnon mode. a_j^{in} and b^{in} are the noise operators for the cavity mode j and magnon mode, respectively. For convenience, we rewrite Eqs. (3) and (4) in a more compact form

$$\frac{da_j}{dt} = -i[a_j, H'] + \sqrt{2\kappa_j}a_j^{\text{in}}, \tag{5}$$

$$\frac{db}{dt} = -i[b, H'] + \sqrt{2\gamma}b^{\text{in}}, \tag{6}$$

with the new Hamiltonian being

$$H' = \sum_{j=1,2}\Big[P_j a_j^\dagger a_j + g_j(a_j b^\dagger + a_j^\dagger b) + \frac{G_j}{2}(a_j a_j + \text{H.c.})\Big] + Qb^\dagger b + \frac{K}{2} b^\dagger b^\dagger b b. \tag{7}$$

According to Refs. [36,59], the parity operator for our double-cavity magnonic system can be defined by $\Pi = e^{i\pi(\sum_{j=1,2} a_j^\dagger a_j + b^\dagger b)}$. It is easy to validate that the non-Hermitian Hamiltonian H' commutes with the parity operator Π. This implies that the parity determined by the excitation number (i.e., $\sum_{j=1,2} a_j^\dagger a_j + b^\dagger b$) is preserved in the double-cavity magnonic system. In general, the excitation number can be any natural number. When it takes the numbers $0, 2, 4, \ldots$ or $1, 3, 5, \ldots$, we say that the system is parity symmetric. When it takes some continuous values like $0, 1, 2, 3, \ldots$, we call that the parity symmetry of the system is broken.

To study the steady-state properties of the system, we express the operator as the sum of the expectation value and its fluctuation, i.e., $a_j = \langle a_j\rangle + \delta a_j$ and $b = \langle b\rangle + \delta b$. With the help of these expansions, we can obtain the dynamical equations for the expectation values:

$$\frac{d\langle a_j\rangle}{dt} = -iP_j\langle a_j\rangle - iG_j\langle a_j^\dagger\rangle - ig_j\langle b\rangle, \tag{8}$$

$$\frac{d\langle b\rangle}{dt} = -i(Q + U_1)\langle b\rangle - ig_1\langle a_1\rangle - ig_2\langle a_2\rangle, \tag{9}$$

where $U_1 = K\langle b^\dagger\rangle\langle b\rangle$. In Eqs. (8) and (9) we have assumed that the expectation values of both the noise and fluctuation

operators are zero. The dynamical equations for the fluctuation operators and the mean correlated fluctuations are given in Appendix B.

Based on Eqs. (8) and (9) and using the approximation $\langle b^\dagger b\rangle \approx \langle b^\dagger\rangle\langle b\rangle$, we can find three solutions for the mean magnon number, which are

$$\langle b^\dagger b\rangle_0 = 0, \quad \langle b^\dagger b\rangle_\pm = \frac{-\Delta \pm \sqrt{-\Gamma^2 + (\xi_1 G_1 + \xi_2 G_2)^2}}{K}, \tag{10}$$

where $\Delta = \Delta_b - (\xi_1\Delta_1 + \xi_2\Delta_2)$, $\Gamma = \gamma + \xi_1\kappa_1 + \xi_2\kappa_2$, and $\xi_j = g_j^2/(\Delta_j^2 - G_j^2 + \kappa_j^2)$. Now we analyze the stability of the solutions $\langle b^\dagger b\rangle_{0,\pm}$. The dynamical equations for the fluctuation operators are

$$\frac{d\delta\boldsymbol{r}}{dt} = \boldsymbol{O}\cdot\delta\boldsymbol{r} + \delta\boldsymbol{r}^{\rm in}, \tag{11}$$

where $\delta\boldsymbol{r} = (\delta a_1, \delta a_2, \delta b, \delta a_1^\dagger, \delta a_2^\dagger, \delta b^\dagger)^T$ and $\delta\boldsymbol{r}^{\rm in} = (\sqrt{2\kappa_1}a_1^{\rm in}, \sqrt{2\kappa_2}a_2^{\rm in}, \sqrt{2\gamma}b^{\rm in}, \sqrt{2\kappa_1}a_1^{\rm in\dagger}, \sqrt{2\kappa_2}a_2^{\rm in\dagger}, \sqrt{2\gamma}b^{\rm in\dagger})^T$. The matrix $\boldsymbol{O}$ is

$$\boldsymbol{O} = \begin{pmatrix} -iP_1 & 0 & -ig_1 & -iG_1 & 0 & 0 \\ 0 & -iP_2 & -ig_2 & 0 & -iG_2 & 0 \\ -ig_1 & -ig_2 & -i(Q+2U_1) & 0 & 0 & -iU_2 \\ iG_1 & 0 & 0 & iP_1^* & 0 & ig_1 \\ 0 & iG_2 & 0 & 0 & iP_2^* & ig_2 \\ 0 & 0 & iU_2^* & ig_1 & ig_2 & i(Q^*+2U_1) \end{pmatrix}, \tag{12}$$

where $U_2 = K\langle b\rangle^2$.

By calculating the determinant $|\lambda\boldsymbol{I} - \boldsymbol{O}| = 0$ with $\boldsymbol{I}$ being the identity matrix, the eigenvalues (i.e., λ) of the matrix $\boldsymbol{O}$ can be obtained. The stability of the solutions $\langle b^\dagger b\rangle_{0,\pm}$ is determined by the values of Re[λ] [60]. When all the values of Re[λ] are negative, the solution is stable. When one of these values is positive, the solution is unstable. The analysis of Re[λ] demonstrates that the solution $\langle b^\dagger b\rangle_-$ is unstable in the whole parameter space, while the solutions $\langle b^\dagger b\rangle_0$ and $\langle b^\dagger b\rangle_+$ are stable in some parameter space. Subsequently, to study the steady-state quantum phase transitions, we only need to consider the solutions $\langle b^\dagger b\rangle_0$ and $\langle b^\dagger b\rangle_+$.

We use the mean magnon number (i.e., $\langle b^\dagger b\rangle \geqslant 0$) as an order parameter of the phase transition and the properties of the system change fundamentally at a specific driving strength of cavity C1. This driving strength is the critical point of the phase transition and we denote it as $G_1 = G_{p,q}$. The number of the critical points depends on Δ_b/Δ_1. For convenience, we introduce a parameter η (to be defined later) and then the critical driving strength can be expressed as follows.

(i) For $\Delta_b/\Delta_1 < \eta$, there are two critical driving strengths, which are

$$\begin{aligned} G_p &= \frac{g_1^2\alpha_1 - \alpha_2}{2(\alpha_3 - \gamma\alpha_1)} \\ G_q &= \frac{\alpha_4 - g_1^2 g_2^2 G_2}{\alpha_5}, \end{aligned} \tag{13}$$

with $\eta = \{g_1^2\alpha_1 + \alpha_2 + 2[g_2^2(\alpha_6 - \kappa_1 G_2) + \gamma\kappa_1\alpha_1]\}/(2\Delta_1^2\alpha_1)$. For simplicity, we have used the parameters $\alpha_1 = \Delta_2^2 - G_2^2 + \kappa_2^2$, $\alpha_2 = [g_1^4\alpha_1^2 + 4(\alpha_3 - \gamma\alpha_1)(\alpha_3\beta_3 - \alpha_1\beta_2)]^{1/2}$, $\alpha_3 = g_2^2(G_2 - \kappa_2)$, $\alpha_4 = \{\alpha_5[\alpha_5\beta_3 + 2g_1^2(g_2^2\alpha_6 - \alpha_1\beta_1) + g_1^4\alpha_1] + g_1^4 g_2^4 G_2^2\}^{1/2}$, $\alpha_5 = 2g_2^2(\gamma\kappa_2 - \Delta_2\Delta_b) + (\gamma^2 + \Delta_b^2)\alpha_1 + g_2^4$, and $\alpha_6 = \Delta_1\Delta_2 + \kappa_1\kappa_2$, where $\beta_1 = \Delta_1\Delta_b - \gamma\kappa_1$, $\beta_2 = \gamma\Delta_1^2 + \kappa_1(\gamma\kappa_1 + g_1^2)$, and $\beta_3 = \Delta_1^2 + \kappa_1^2$.

When $G_1 < G_p$, $\langle b^\dagger b\rangle = \langle b^\dagger b\rangle_0$. When $G_p < G_1 < G_q$, $\langle b^\dagger b\rangle$ can be $\langle b^\dagger b\rangle_0$ or $\langle b^\dagger b\rangle_+$. When $G_1 > G_q$, $\langle b^\dagger b\rangle = \langle b^\dagger b\rangle_+$. In the vicinity of the critical point G_q, we find that the relation between $\langle b^\dagger b\rangle$ and $|G_1 - G_q|$ follows:

$$\langle b^\dagger b\rangle \simeq |G_1 - G_q|^\nu, \tag{14}$$

where $\nu = 1$ is the dynamical critical exponent of the phase transition.

(ii) For $\Delta_b/\Delta_1 = \eta$, the two critical driving strengths become equal, i.e., $G_p = G_q$.

(iii) For $\Delta_b/\Delta_1 > \eta$, the critical driving strength is G_q. In this case, $\langle b^\dagger b\rangle = \langle b^\dagger b\rangle_0$ for $G_1 < G_q$ while $\langle b^\dagger b\rangle = \langle b^\dagger b\rangle_+$ for $G_1 > G_q$.

The two critical points $G_{p,q}$ and one critical exponent ν obtained above give key information about the phase transitions of the system. In the next section we will focus on the characteristics and controllability of the QPT. To this end, we regard the cavity C1 as a main cavity and denote the cavity C2 as an auxiliary cavity. This distinction makes it clear that the main cavity is used to observe the phase transitions and the secondary cavity is used to control them. It should be emphasized that both the driving of the cavity and the Kerr nonlinearity for the magnon are important for the phase transitions of the system. Here we only pay attention to the situation with $g_1 g_2 \neq 0$ and $G_j < \sqrt{\Delta_j^2 + \kappa_j^2}$, because when $g_j = 0$ and $G_j > \sqrt{\Delta_j^2 + \kappa_j^2}$ the two cavities are unstable [36,56]. In the calculations, we set the parameter values of the main cavity (except for G_1/κ_1) as $\Delta_1/\kappa_1 = 3$, $g_1/\kappa_1 = 2.4$, and $\gamma/\kappa_1 = 1$. This choice ensures that the parameters are consistent with those of the single-cavity magnonic system [36].

III. CONTROLLABLE QUANTUM PHASE TRANSITION

In this section, we explore the influence of the auxiliary cavity on the phase transitions of the main cavity. First, we present the phase diagrams of the main cavity for three sets of parameters of the auxiliary cavity as shown in Figs. 2(a)–2(c). In each phase diagram, there are three different phases, i.e., PSP, PSBP, and BP. The orange solid curve and the vertical violet solid line correspond to the critical points $G_1 = G_q$ and $G_1 = G_p$, respectively. We can clearly see that the boundary between PSP and PSBP is given by $G_1 = G_q$ when $\Delta_b/\Delta_1 > \eta$. The boundary between PSP and BP is determined by $G_1 = G_p$ when $\Delta_b/\Delta_1 < \eta$. When $\Delta_b/\Delta_1 = \eta$, we introduce a new notation G to present the critical driving strength due to the indistinguishable nature of $G_{p,q}$, i.e., $G_1 = G_p = G_q = G$. The values of the critical point G/κ_1 in Figs. 2(a), 2(b), and 2(c) are 0.8031, 1.4612, and 2.0479, respectively. Obviously, the value of G given in our system can be larger or smaller than that (i.e., $G/\kappa_1 = 2.024$) in the single-cavity magnonic system [36]. The above results imply that the phase transitions of the system are controllable. The controllability is reflected in the fact that the critical point can be shifted flexibly, which is beneficial for experimental observation.

Furthermore, we show the dynamical behaviors of the mean magnon number $\langle b^\dagger b\rangle/(\gamma/K)$ for different phases by

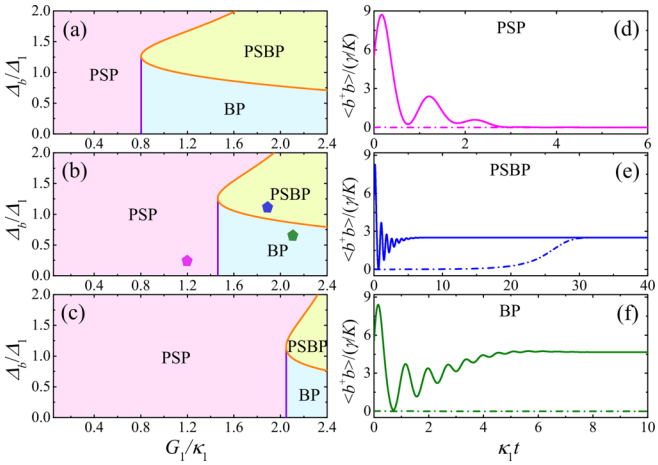

FIG. 2. Left column: Phase diagram of the double-cavity magnonic system. Right column: Dynamical behaviors of the mean magnon number for three phases [the corresponding parameters have been marked in (b)]. (a) $(\kappa_2, \Delta_2, g_2, G_2)/\kappa_1 = (0.5, 2.6, 1.5, 2)$, (b) $(\kappa_2, \Delta_2, g_2, G_2)/\kappa_1 = (0.6, 3.1, 1.8, 1.9)$, and (c) $(\kappa_2, \Delta_2, g_2, G_2)/\kappa_1 = (1.1, 3.5, 1.3, 0.8)$. (d) $(\Delta_b/\Delta_1, G_1/\kappa_1) = (0.2, 1.2)$ for PSP, (e) $(\Delta_b/\Delta_1, G_1/\kappa_1) = (1.1, 1.9)$ for PSBP, and (f) $(\Delta_b/\Delta_1, G_1/\kappa_1) = (0.7, 2.1)$ for BP. The initial conditions for the dashed lines in (d), (e), and (f) are $(\langle a_j\rangle, \langle b\rangle)/\sqrt{\gamma/K} = (0.04 + 0.07i, 0.04 - 0.07i)$ while the initial conditions for the solid lines are $(\langle a_j\rangle, \langle b\rangle)/\sqrt{\gamma/K} = (1.8 + 1.5i, 1.8 - 1.5i)$.

Figs. 2(d)–2(f). Notice that we have rescaled $\langle b^\dagger b\rangle$ in terms of γ/K which can be viewed as a system-size parameter (which could be determined also by the parameters of the cavities) according to Ref. [61]. The advantage of this choice is that we can limit the mean magnon number to less than 10 to illustrate the results clearly. The parameters for each phase have been marked in Fig. 2(b). Figure 2(d) illustrates the dynamics of the system for PSP. In this phase, we see that only the solution $\langle b^\dagger b\rangle_0$ is stable. The excitation number is zero and thus the system is parity symmetric. When the system is in PSBP as shown in Fig. 2(e), it is found that only the solution $\langle b^\dagger b\rangle_+$ is stable. The excitation number in this case takes the continuous value and thus the system is parity-symmetry broken. However, when the system is in BP [see Fig. 2(f)], both the solutions $\langle b^\dagger b\rangle_+$ and $\langle b^\dagger b\rangle_0$ are stable, which implies that in this case the parity symmetry can be conserved or broken.

The results presented in Fig. 2 suggest that if we want to identify the three phases by the dynamical behaviors, we must track the dynamics of two different initial states which correspond to two sets of different initial conditions (one set is close to zero and the other set is far away from zero). However, when we only track the dynamics of an initial state near zero, PSB and BP cannot be distinguished since the solution $\langle b^\dagger b\rangle_0$ is stable for both phases. In this situation, to distinguish the two phases and observe the phase transition clearly, we need to add additional driving pulses to the system. In principle, the driving pulse can be added to the main cavity or the auxiliary cavity or both cavities because it does not affect the results. The main intention of this paper is to control the phase transition of the main cavity by adjusting the parameters of the auxiliary cavity. Therefore, we only

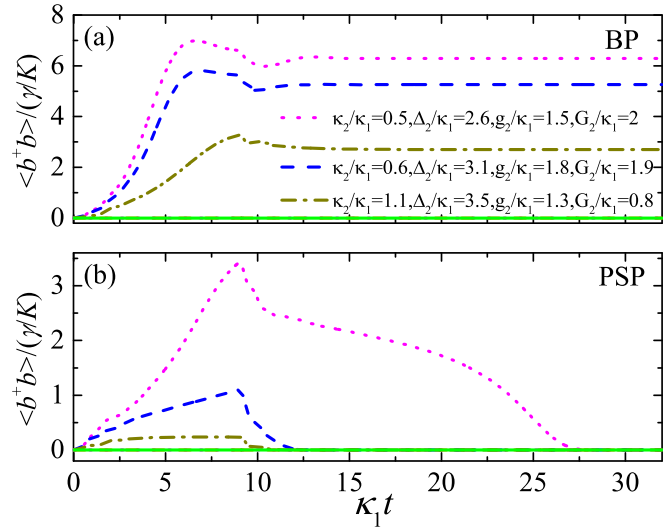

FIG. 3. Dynamical behaviors of the mean magnon number $\langle b^\dagger b\rangle/(\gamma/K)$ for two phases: (a) BP with $G_1/\kappa_1 = 2.1$ and (b) PSP with $G_1/\kappa_1 = 0.7$. Broken lines show the results with the additional pulse and solid lines give the results without the pulse field. The initial conditions are $(\langle a_j\rangle, \langle b\rangle) = (0, 0)$. Other parameters are $\Delta_b/\Delta_1 = 0.5$, $\Omega_0/\kappa_1\sqrt{\gamma/K} = 2.2$, and $\kappa_1\tau = 9$.

add the additional pulse to the auxiliary cavity. The shape of the pulse is governed by the form of Rabi frequency, i.e., $\Omega(t) = \Theta(\tau - t)\Omega_0 \cos[\pi t/(2\tau)]$, where $\Theta(\tau - t)$ indicates the Heaviside function and Ω_0 is the initial Rabi frequency [36]. When the driving pulse is taken into account, we can rewrite the dynamical equation (8) as

$$\frac{d\langle a_j\rangle}{dt} = -iP_j\langle a_j\rangle - iG_j\langle a_j^\dagger\rangle - ig_j\langle b\rangle - i\Omega(t)\delta_{j,2}, \quad (15)$$

where $\delta_{j,2}$ denotes the delta function with $j = 1$ and 2. To verify the effectiveness of the strategy proposed above, for both phases PSP and BP, we evolve the system according to Eqs. (15) and (9) from an initial state $(\langle a_j\rangle, \langle b\rangle) = (0, 0)$. The results about the dynamical behaviors of the mean magnon number for BP and PSP are shown in Figs. 3(a) and 3(b), respectively. For each phase, we demonstrate the results for three sets of parameters of the auxiliary cavity. For the same initial state, we see that the system eventually stabilizes to the steady state $\langle b^\dagger b\rangle_+$ for BP while the system finally stabilizes to the steady state $\langle b^\dagger b\rangle_0$ for PSP. The same initial state leads to different final states, which makes it easy to distinguish the two phases based on the different dynamical behaviors. For comparison, we also show the results (see solid lines) without additional pulse field in Fig. 3. In this case, we see that the system eventually stabilizes to the unique steady state $\langle b^\dagger b\rangle_0$ for both phases and thus the two phases are indistinguishable.

We have explored the three phases of the system and their dynamical characteristics above. In the following part, we will study the influence of the parameters of the auxiliary cavity on the critical point of the phase transition of the main cavity, which is very important for the experimental observation of the phase transition. We focus on the critical case where $\Delta_b/\Delta_1 = \eta$. In this case the critical point of the phase transitions is given by the critical driving strength G

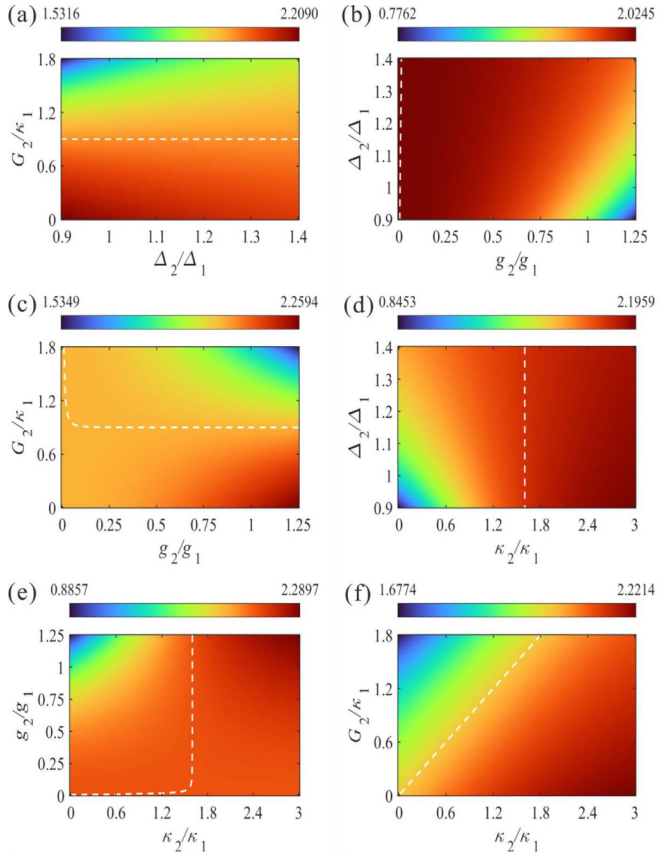

FIG. 4. Contour plot of the critical driving strength G/κ_1 shown in different parameter planes. The parameter planes are spanned by (a) $(\Delta_2/\Delta_1, G_2/\kappa_1)$ with $(\kappa_2, g_2)/\kappa_1 = (0.9, 1.8)$, (b) $(g_2/g_1, \Delta_2/\Delta_1)$ with $(\kappa_2, G_2)/\kappa_1 = (0.9, 1.6)$, (c) $(g_2/g_1, G_2/\kappa_1)$ with $(\kappa_2, \Delta_2)/\kappa_1 = (0.9, 4)$, (d) $(\kappa_2/\kappa_1, \Delta_2/\Delta_1)$ with $(g_2, G_2)/\kappa_1 = (1.8, 1.6)$, (e) $(\kappa_2/\kappa_1, g_2/g_1)$ with $(\Delta_2, G_2)/\kappa_1 = (4, 1.6)$, and (f) $(\kappa_2/\kappa_1, G_2/\kappa_1)$ with $(\Delta_2, g_2)/\kappa_1 = (4, 1.8)$, respectively. White lines mark the critical value obtained in the single-cavity magnonic system [36].

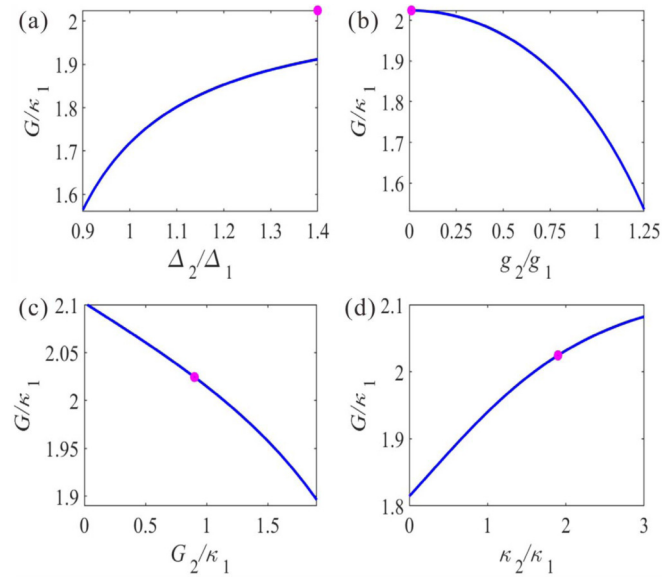

FIG. 5. Critical driving strength G/κ_1 as a function of the parameters (a) Δ_2/Δ_1 with $(\kappa_2, g_2, G_2)/\kappa_1 = (0.9, 1.6, 1.9)$, (b) g_2/g_1 with $(\kappa_2, \Delta_2, G_2)/\kappa_1 = (0.9, 4, 1.8)$, (c) G_2/κ_1 with $(\kappa_2, \Delta_2, g_2)/\kappa_1 = (0.9, 4, 1.6)$, and (d) κ_2/κ_1 with $(\Delta_2, g_2, G_2)/\kappa_1 = (4, 1.4, 1.9)$, respectively. Magenta points mark the critical driving strength given by the single-cavity magnonic model [36].

as defined before. For simplicity, in our calculations we scale the parameters of the auxiliary cavity by the corresponding parameters of the main cavity, i.e., κ_2/κ_1, g_2/g_1, Δ_2/Δ_1, and G_2/κ_1. Considering that the auxiliary cavity has four parameters that can be adjusted, for convenience we combine these parameters into six groups and then see the change of the critical driving strength in the plane spanned by each group of parameters. Figure 4 shows the contour plot of the critical point G/κ_1 in six parameter planes. Different colors indicate different values of the critical driving strength G/κ_1. For comparison, we mark the critical driving strength obtained in the single-cavity magnonic system [36] by white lines. We find that except for Fig. 4(b), the white lines are located in the middle of the parameter planes, which implies that the value of G/κ_1 in these figures can be either greater than or less than the critical driving strength obtained in the single-cavity magnonic system [36]. In some parameter regions, we see that a slight change in the parameters can leads to a great change of G/κ_1. These results indicate that the critical point of the phase transformation of the main cavity can be flexibly adjusted by introducing the auxiliary cavity. In particular, the adjustments of some parameters of the auxiliary cavity can significantly reduce the critical driving intensity (see dark blue regions), which is beneficial for experimental observations.

In Fig. 5, we further show the dependence of the phase transition point of the main cavity on the single parameter of the auxiliary cavity. It can be seen that the critical driving strength of the phase transition decreases obviously with the decrease of both the detuning and dissipation of the auxiliary cavity [see Figs. 5(a) and 5(d)]. As the coupling between the auxiliary cavity and the magnon or the driving of the auxiliary cavity increases, we also see that the critical driving strength of the main cavity decreases rapidly or even decreases by an order of magnitude [see Fig. 5(b) or 5(c)]. These findings indicate that the strategy of introducing auxiliary cavity can make it easier to observe the QPT of the system experimentally. In other words, the phase transition of the system is highly controllable. To determine the order of phase transitions, we study the behavior of the order parameter: Mean magnon number $\langle b^\dagger b\rangle$ especially its behavior near the critical point based on both analytical and numerical methods. Here we consider three cases in which $\Delta_b/\Delta_1 < \eta$, $\Delta_b/\Delta_1 = \eta$, and $\Delta_b/\Delta_1 > \eta$. The corresponding results are demonstrated by Figs. 6(a), 6(b), and 6(c). For each case, we obtain the results for three sets of auxiliary-cavity parameters. In Fig. 6(a), $\Delta_b/\Delta_1 < \eta$, the critical driving strength is $G_1 = G_p$. The region for $G_1 < G_p$ denotes PSP (the mean magnon number is zero), the region for $G_1 > G_p$ denotes BP. Because in BP both $\langle b^\dagger b\rangle_0$ and $\langle b^\dagger b\rangle_+$ are stable, the steady-state mean magnon number in this case is determined by the initial conditions. When the initial condition is close to zero, the final mean magnon number is zero, which is indistinguishable from PSP. In this situation, as mentioned earlier (see Fig. 3), we must add a pulse field to induce the system to the nonzero state to

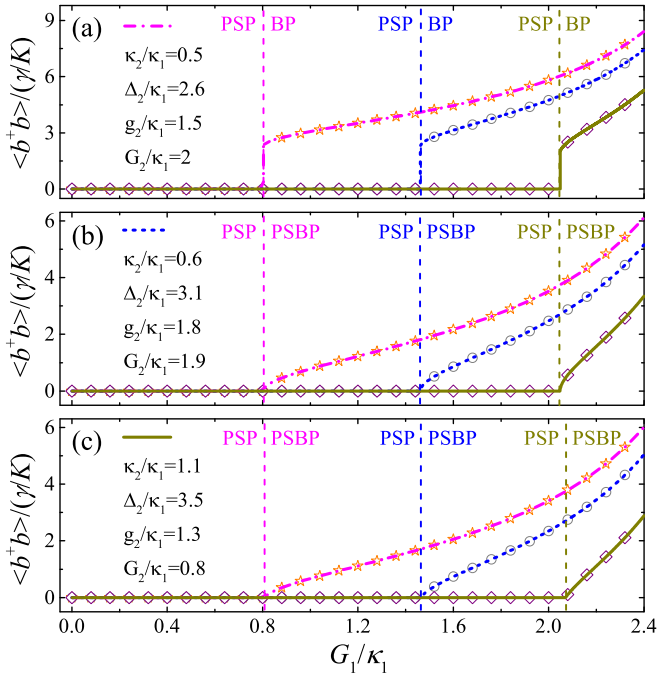

FIG. 6. Mean magnon number $\langle b^\dagger b\rangle/(\gamma/K)$ as a function of the driving strength G_1/κ_1 for (a) $\Delta_b/\Delta_1 = 0.5$, (b) $\Delta_b/\Delta_1 = \eta$, and (c) $\Delta_b/\Delta_1 = 1.3$. Lines present our analytical results given by Eq. (10) while scatters show the numerical results obtained from Eqs. (15) [or (8)] and (9). Vertical dashed lines mark the locations of the critical driving strength, in both (a) and (b) they are (from left to right) 0.8031, 1.4612, and 2.0479, while in (c) they are (from left to right) 0.8080, 1.4653, and 2.0704. The parameters $(\kappa_2, \Delta_2, g_2, G_2)/\kappa_1$ are (0.5,2.6,1.5,2), (0.6,3.1,1.8,1.9), and (1.1,3.5,1.3,0.8) for the results denoted by magenta, blue, and dark yellow colors, respectively. $\Omega_0/\kappa_1\sqrt{\gamma/K} = 2.2$ and $\kappa_1\tau = 9$ are used in (a).

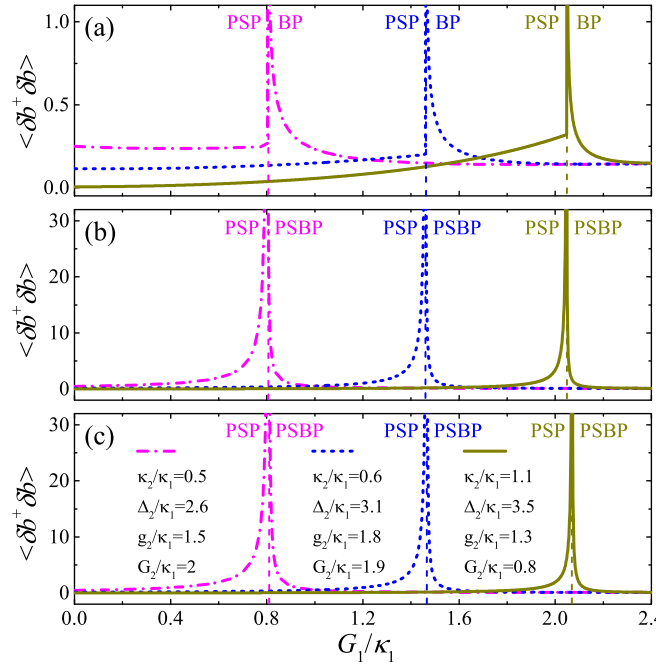

FIG. 7. Mean correlated fluctuation $\langle\delta b^\dagger\delta b\rangle$ as a function of the driving strength G_1/κ_1 for (a) $\Delta_b/\Delta_1 = 0.5$, (b) $\Delta_b/\Delta_1 = \eta$, and (c) $\Delta_b/\Delta_1 = 1.3$. Vertical dashed lines mark the locations of the critical driving strength. All parameters are the same as in Fig. 6.

distinguish BP from PSP. We find that in the vicinity of the critical point G_p, the mean magnon number has an obvious jumping behavior, which implies that the system experiences a first-order phase transition from PSP to BP. In Fig. 6(b), $\Delta_b/\Delta_1 = \eta$, the critical driving strength is $G_1 = G$. When $G_1 < G$, the system is in PSP (the mean magnon number is zero). When $G_1 = G$, the system is in three-phase coexistence. When $G_1 > G$, the system is in PSBP (the mean magnon number is nonzero). In Fig. 6(c), $\Delta_b/\Delta_1 > \eta$, the critical driving strength is $G_1 = G_q$. When $G_1 < G_q$, the mean magnon number is zero, which illustrates that the system is in PSP. When $G_1 > G_q$, the mean magnon number is nonzero, which implies that the system is in PSBP. In the vicinity of $G_1 = G_q$, we see that the mean magnon number varies continuously, which confirms that the system experiences a second-order phase transition from PSP to PSBP.

Finally, we investigate the behavior of the mean correlated fluctuation $\langle\delta b^\dagger\delta b\rangle$ which can be used to characterize the QPT of the system. Similar to Fig. 6, Fig. 7 also shows the results for three cases $\Delta_b/\Delta_1 < \eta$, $\Delta_b/\Delta_1 = \eta$, and $\Delta_b/\Delta_1 > \eta$. In Fig. 7(a), $\Delta_b/\Delta_1 < \eta$, we see a catastrophic divergent behavior of the mean correlated fluctuation in the vicinity of the critical point $G_1 = G_p$, which corresponds to the first-order QPT from PSP to BP. However, in Fig. 7(c), $\Delta_b/\Delta_1 > \eta$, we see an asymptotic divergent behavior of the mean correlated fluctuation in the vicinity of the critical point $G_1 = G_q$, which corresponds to the second-order QPT from PSP to PSBP. Figure 7(b) shows the critical case $\Delta_b/\Delta_1 = \eta$ in which $G_1 = G$, the behavior of the mean correlated fluctuation in this case is between the behaviors in Figs. 7(a) and 7(c). In each case, similar behavior is shown for three different sets of auxiliary-cavity parameters. All our results for the mean correlated fluctuation are obtained by numerically calculating the quantity X_{11} (for details please see Appendix B).

IV. DISCUSSIONS AND CONCLUSIONS

Compared with the single-cavity magnonic system [36], our double-cavity magnonic system has some advantages. First, the two types of quantum phase transitions obtained in the single-cavity magnonic system have been exhibited in our system. Moreover, with the introducing of the auxiliary cavity, the quantum phase transitions of the system become more controllable. Second, the double-cavity magnonic model presented in this paper can be realized in experiment. Furthermore, the phase transitions of our system are easier to be observed experimentally due to their high controllability. Now we analyze the experimental feasibility. According to Ref. [62], $\kappa_1/2\pi = 2.04$ MHz. The critical driving strengths in Figs. 2(a), 2(b), and 2(c) (0.8031, 1.4612, and 2.0479) become 1.6383, 2.9808, and 4.1777 MHz, which are in the range $0 < G_1/2\pi < 6$ MHz allowed by the experiment [36,63]. In Figs. 3–7, the maximum critical driving strength is located at $(G/\kappa_1 = 2.2897)$ [see Fig. 4(e)] 4.6710 MHz, which is also in the range allowed by the experiment. In addition, the parameters of the main cavity in our system are consistent

with those in Ref. [36] and all our selected parameters can be reached in experiment.

To summarize, we have studied the controllable quantum phase transitions in a double-cavity magnonic system. It is shown that the system experiences a second-order phase transition from a parity-symmetric phase to a parity-symmetry-broken phase and a first-order phase transition from a parity-symmetric phase to a bistable phase when the driving strength of one cavity is above a critical value. We have obtained the phase diagram, the critical point, and the corresponding critical exponent to characterize the phase transitions. It is found that the critical driving strength in our system can be either greater than or less than that obtained in a single-cavity magnonic system [36]. We have demonstrated a wide adjustable range of the critical driving strength, which provides a favorable theoretical support for experimental observation of the phase transitions. We have investigated the behaviors of both mean magnon number and mean correlation fluctuation with respect to the driving strength of the main cavity, which can be used to verify the controllable phase transitions. We expect our present work will be implemented experimentally in the future.

ACKNOWLEDGMENTS

Y.Q. appreciates many helpful discussions with G.-Q. Zhang. This work was supported by the National Natural Science Foundation of China (Grant No. 11974273).

APPENDIX A: MODELING OF THE DOUBLE-CAVITY MAGNONIC SYSTEM

In this Appendix, we give the modeling process of the double-cavity magnonic system in detail. The total Hamiltonian of this system reads as ($\hbar = 1$)

$$H = \sum\nolimits_{j=1,2}(H_{a,j} + H_{\mathrm{int},j} + H_{d,j}) + H_b, \tag{A1}$$

where $H_{a,j}$ in Eq. (A1) is the Hamiltonian of the cavity mode j, i.e.,

$$H_{a,j} = \omega_j a_j^\dagger a_j. \tag{A2}$$

In our scheme, both cavities are driven by the external driving field, the corresponding Hamiltonian is given by [36,61]

$$H_{d,j} = \frac{G_j}{2}(a_j a_j + \mathrm{H.c.})(e^{-i\omega t} + e^{i\omega t}). \tag{A3}$$

The Hamiltonian of the magnon mode can be written as the following form which involved the Zeeman energy and the magnetocrystalline anisotropic energy [43,51,64]

$$H_b = -\int_{V_b} \boldsymbol{M}\cdot\boldsymbol{B}_0 d\tau - \frac{\mu_0}{2}\int_{V_b} \boldsymbol{M}\cdot\boldsymbol{H}_{\mathrm{an}} d\tau, \tag{A4}$$

where $\boldsymbol{M} = (M_x, M_y, M_z)$ is the magnetization of the yttrium iron garnet (YIG) sphere, μ_0 is the vacuum permeability, $\boldsymbol{B}_0 = B_0\boldsymbol{e}_z$ is the magnetic field along the z direction, and V_b is the volume of the YIG sphere. In the case where the magnetic field $\boldsymbol{B}_0$ is aligned along the crystallographic axis [100] of the YIG, the anisotropic field $\boldsymbol{H}_{\mathrm{an}}$ takes the form [65,66]

$$\boldsymbol{H}_{\mathrm{an}} = -\frac{2K_{\mathrm{an}}M_z}{M^2}\boldsymbol{e}_z, \tag{A5}$$

where K_{an} is the first-order anisotropy constant.

Then the Hamiltonian (A4) can be expressed as

$$H_b = -B_0 M_z V_b + \frac{\mu_0 K_{\mathrm{an}} M_z^2 V_b}{M^2}. \tag{A6}$$

After introducing the macrospin operator $\boldsymbol{S} = \boldsymbol{M}V_b/\gamma \equiv (S_x, S_y, S_z)$ [67] with γ as the gyromagnetic ration, Eq. (A6) is rewritten as

$$H_b = -\gamma B_0 S_z + \frac{\mu_0 K_{\mathrm{an}}\gamma^2}{M^2 V_b} S_z^2. \tag{A7}$$

One can obtain the magnon operator by using the Holstein-Primakoff transformation [68]

$$S^+ = (\sqrt{2S - b^\dagger b})b,\ \ S^- = b^\dagger(\sqrt{2S - b^\dagger b}),\ \ S_z = S - b^\dagger b, \tag{A8}$$

where $S^\pm \equiv S_x \pm iS_y$ are the raising and lowering operators of the macrospin and S is the total spin. As a result, Eq. (A7) can be further shown as follows:

$$H_b = \omega_b b^\dagger b + \frac{K}{2} b^\dagger b b^\dagger b = \omega_b' b^\dagger b + \frac{K}{2} b^\dagger b^\dagger b b, \tag{A9}$$

where $\omega_b' = \omega_b + K/2$ with $K = 2\mu_0 K_{\mathrm{an}}\gamma^2/(M^2 V_b)$ and $\omega_b = \gamma B_0 - 2\mu_0 K_{\mathrm{an}}\gamma^2 S/(M^2 V_b)$. Obviously, K is positive in this case. Compared with ω_b, $K/2$ is small and can be neglected, i.e., $\omega_b' \approx \omega_b$. Then Eq. (A9) becomes

$$H_b = \omega_b b^\dagger b + \frac{K}{2} b^\dagger b^\dagger b b. \tag{A10}$$

The Hamiltonian pertaining to the cavity-macrospin interaction is given by [43,67]

$$H_{\mathrm{int},j} = g_{s,j}(a_j + a_j^\dagger)(S^- + S^+), \tag{A11}$$

where $g_{s,j}$ indicates the coupling between the cavity mode j and the macrospin. Under the condition of low-lying excitations, i.e., $\langle b^\dagger b\rangle \ll 2S$, the S^- and S^+ in Eq. (A8) become $S^- \approx b^\dagger\sqrt{2S}$ and $S^+ \approx b\sqrt{2S}$, which results in

$$\begin{aligned} H_{\mathrm{int},j} &= \sqrt{2S}g_{s,j}(a_j + a_j^\dagger)(b + b^\dagger) \\ &= g_j(a_j + a_j^\dagger)(b + b^\dagger), \end{aligned} \tag{A12}$$

where $g_j = \sqrt{2S}g_{s,j}$ indicates the coupling between the cavity mode j and the magnon mode.

Naturally, the Hamiltonian (A1) is obtained as

$$\begin{aligned} H = \sum_{j=1,2}\Big[&\omega_j a_j^\dagger a_j + g_j(a_j + a_j^\dagger)(b + b^\dagger) + \frac{G_j}{2}(a_j a_j + \mathrm{H.c.}) \\ &\times (e^{-i\omega t} + e^{i\omega t})\Big] + \omega_b b^\dagger b + \frac{K}{2} b^\dagger b^\dagger b b. \end{aligned} \tag{A13}$$

One can transform the Hamiltonian (A13) into the interaction picture via adopting the unitary transformation $U' = e^{-i(\sum_{j=1,2}\omega_j a_j^\dagger a_j + \omega_b b^\dagger b)t}$ and $g_j(a_j + a_j^\dagger)(b + b^\dagger) \to g_j(a_j b^\dagger + a_j^\dagger b)$, in which the fast-oscillating terms $g_j a_j^\dagger b^\dagger e^{i(\omega_j + \omega_b)t}$ and $g_j a_j b e^{-i(\omega_j + \omega_b)t}$ can be neglected. The coupling g_j is

sufficiently weak, i.e., $g_j \ll \omega_j$, ω_b. Similarly, the approximation $\frac{G_j}{2}(a_j a_j + \text{H.c.})(e^{-i\omega t} + e^{i\omega t}) \to \frac{G_j}{2}(a_j a_j e^{i\omega t} + \text{H.c.})$ is valid when the fast-oscillating terms $\frac{G_j}{2}a_j^\dagger a_j^\dagger e^{i(2\omega_j+\omega)t}$ and $\frac{G_j}{2}a_j a_j e^{-i(2\omega_j+\omega)t}$ can be neglected. The above uses the well-known rotating-wave approximation [56]. Under the rotating-wave approximation, the Hamiltonian (A13) becomes

$$H = \sum_{j=1,2}\Big[\omega_j a_j^\dagger a_j + g_j(a_j b^\dagger + a_j^\dagger b) + \frac{G_j}{2}(a_j a_j e^{i\omega t} + \text{H.c.})\Big] + \omega_b b^\dagger b + \frac{K}{2}b^\dagger b^\dagger bb. \tag{A14}$$

This is exactly the model we have proposed and used to study the controllable QPT.

APPENDIX B: DYNAMICAL EQUATIONS OF THE MEAN CORRELATED FLUCTUATIONS

The dynamics of the fluctuation operators are described by the following equations:

$$\frac{d\delta a_j}{dt} = -iP_j\delta a_j - iG_j\delta a_j^\dagger - ig_j\delta b + \sqrt{2\kappa_j}a_j^{\text{in}}, \tag{B1}$$

$$\frac{d\delta b}{dt} = -i(Q+2U_1)\delta b - iU_2\delta b^\dagger - ig_1\delta a_1 - ig_2\delta a_2 + \sqrt{2\gamma}b^{\text{in}}. \tag{B2}$$

Among them, the fluctuations's high-order terms have been omitted.

From the above equations, we can obtain the dynamical equations of the mean correlated fluctuations

$$\frac{d\langle\delta a_j^\dagger\delta a_j\rangle}{dt} = -2\kappa_j\langle\delta a_j^\dagger\delta a_j\rangle + iG_j(\langle\delta a_j\delta a_j\rangle - \langle\delta a_j^\dagger\delta a_j^\dagger\rangle) + ig_j(\langle\delta a_j\delta b^\dagger\rangle - \langle\delta a_j^\dagger\delta b\rangle), \tag{B3}$$

$$\frac{d\langle\delta a_j\delta a_j\rangle}{dt} = -2iP_j\langle\delta a_j\delta a_j\rangle - iG_j(1+2\langle\delta a_j^\dagger\delta a_j\rangle) - 2ig_j\langle\delta a_j\delta b\rangle, \tag{B4}$$

$$\frac{d\langle\delta a_1\delta a_2\rangle}{dt} = -i(P_1+P_2)\langle\delta a_1\delta a_2\rangle - i(G_2\langle\delta a_1\delta a_2^\dagger\rangle + G_1\langle\delta a_1^\dagger\delta a_2\rangle) - i(g_2\langle\delta a_1\delta b\rangle + g_1\langle\delta a_2\delta b\rangle), \tag{B5}$$

$$\frac{d\langle\delta a_j\delta b\rangle}{dt} = -i(P_j+Q+2U_1)\langle\delta a_j\delta b\rangle - i(U_2\langle\delta a_j\delta b^\dagger\rangle + G_j\langle\delta a_j^\dagger\delta b\rangle) - i(g_1\langle\delta a_1\delta a_j\rangle + g_2\langle\delta a_j\delta a_2\rangle + g_j\langle\delta b\delta b\rangle), \tag{B6}$$

$$\frac{d\langle\delta a_1\delta a_2^\dagger\rangle}{dt} = -i(P_1-P_2^*)\langle\delta a_1\delta a_2^\dagger\rangle + i(G_2\langle\delta a_1\delta a_2\rangle - G_1\langle\delta a_1^\dagger\delta a_2^\dagger\rangle) + i(g_2\langle\delta a_1\delta b^\dagger\rangle - g_1\langle\delta a_2^\dagger\delta b\rangle), \tag{B7}$$

$$\frac{d\langle\delta a_j\delta b^\dagger\rangle}{dt} = -i(P_j-Q^*-2U_1)\langle\delta a_j\delta b^\dagger\rangle + i(U_2^*\langle\delta a_j\delta b\rangle - G_j\langle\delta a_j^\dagger\delta b^\dagger\rangle) + i(g_1\langle\delta a_1^\dagger\delta a_j\rangle + g_2\langle\delta a_2^\dagger\delta a_j\rangle - g_j\langle\delta b^\dagger\delta b\rangle), \tag{B8}$$

$$\frac{d\langle\delta b^\dagger\delta b\rangle}{dt} = -2\gamma\langle\delta b^\dagger\delta b\rangle + i(U_2^*\langle\delta b\delta b\rangle - U_2\langle\delta b^\dagger\delta b^\dagger\rangle) + ig_1(\langle\delta a_1^\dagger\delta b\rangle - \langle\delta a_1\delta b^\dagger\rangle) + ig_2(\langle\delta a_2^\dagger\delta b\rangle - \langle\delta a_2\delta b^\dagger\rangle), \tag{B9}$$

$$\frac{d\langle\delta b\delta b\rangle}{dt} = -2i(Q+2U_1)\langle\delta b\delta b\rangle - iU_2(1+2\langle\delta b^\dagger\delta b\rangle) - 2i(g_1\langle\delta a_1\delta b\rangle + g_2\langle\delta a_2\delta b\rangle). \tag{B10}$$

For simplicity, we define $X_1 \equiv \langle\delta a_1^\dagger\delta a_1\rangle$, $X_2 \equiv \langle\delta a_1\delta a_1\rangle$, $X_3 \equiv \langle\delta a_2^\dagger\delta a_2\rangle$, $X_4 \equiv \langle\delta a_2\delta a_2\rangle$, $X_5 \equiv \langle\delta a_1\delta a_2\rangle$, $X_6 \equiv \langle\delta a_1\delta b\rangle$, $X_7 \equiv \langle\delta a_2\delta b\rangle$, $X_8 \equiv \langle\delta a_1\delta a_2^\dagger\rangle$, $X_9 \equiv \langle\delta a_1\delta b^\dagger\rangle$, $X_{10} \equiv \langle\delta a_2\delta b^\dagger\rangle$, $X_{11} \equiv \langle\delta b^\dagger\delta b\rangle$, and $X_{12} \equiv \langle\delta b\delta b\rangle$. Then, the dynamical equations of the mean correlated fluctuations become

$$\frac{dX_1}{dt} = -2\kappa_1 X_1 + iG_1(X_2 - X_2^*) + ig_1(X_9 - X_9^*), \tag{B11}$$

$$\frac{dX_2}{dt} = -2iP_1X_2 - iG_1(1+2X_1) - 2ig_1X_6, \tag{B12}$$

$$\frac{dX_3}{dt} = -2\kappa_2 X_3 + iG_2(X_4 - X_4^*) + ig_2(X_{10} - X_{10}^*), \tag{B13}$$

$$\frac{dX_4}{dt} = -2iP_2X_4 - iG_2(1+2X_3) - 2ig_2X_7, \tag{B14}$$

$$\frac{dX_5}{dt} = -i(P_1+P_2)X_5 - i(G_2X_8 + G_1X_8^*) - i(g_2X_6 + g_1X_7), \tag{B15}$$

$$\frac{dX_6}{dt} = -i(P_1+Q+2U_1)X_6 - i(U_2X_9 + G_1X_9^*) - i(g_1X_2 + g_2X_5 + g_1X_{12}), \tag{B16}$$

$$\frac{dX_7}{dt} = -i(P_2+Q+2U_1)X_7 - i(U_2X_{10} + G_2X_{10}^*) - i(g_1X_5 + g_2X_4 + g_2X_{12}), \tag{B17}$$

$$\frac{dX_8}{dt} = -i(P_1-P_2^*)X_8 + i(G_2X_5 - G_1X_5^*) + i(g_2X_9 - g_1X_{10}^*), \tag{B18}$$

$$\frac{dX_9}{dt} = -i(P_1-Q^*-2U_1)X_9 + i(U_2^*X_6 - G_1X_6^*) + i(g_1X_1 + g_2X_8 - g_1X_{11}), \tag{B19}$$

$$\frac{dX_{10}}{dt} = -i(P_2-Q^*-2U_1)X_{10} + i(U_2^*X_7 - G_2X_7^*) + i(g_1X_8^* + g_2X_3 - g_2X_{11}), \tag{B20}$$

$$\frac{dX_{11}}{dt} = -2\gamma X_{11} + i(U_2^* X_{12} - U_2 X_{12}^*) + ig_1(X_9^* - X_9) + ig_2(X_{10}^* - X_{10}), \tag{B21}$$

$$\frac{dX_{12}}{dt} = -2i(Q + 2U_1)X_{12} - iU_2(1 + 2X_{11}) - 2i(g_1 X_6 + g_2 X_7). \tag{B22}$$

[1] S. Sachdev, *Quantum Phase Transition* (Cambridge University Press, Cambridge, 1999).

[2] R. Schützhold and G. Schaller, Adiabatic quantum algorithms as quantum phase transitions: First versus second order, Phys. Rev. A **74**, 060304(R) (2006).

[3] S. L. Sondhi, S. M. Girvin, J. P. Carini, and D. Shahar, Continuous quantum phase transitions, Rev. Mod. Phys. **69**, 315 (1997).

[4] M. Vojta, Quantum phase transitions, Rep. Prog. Phys. **66**, 2069 (2003).

[5] D. V. Shopova and D. I. Uzunov, Some basic aspects of quantum phase transitions, Phys. Rep. **379**, 1 (2003).

[6] J. Lang, B. Frank, and J. C. Halimeh, Dynamical Quantum Phase Transitions: A Geometric Picture, Phys. Rev. Lett. **121**, 130603 (2018).

[7] A. A. Zvyagin, Dynamical quantum phase transitions, Low Temp. Phys. **42**, 971 (2016).

[8] P. Jurcevic, H. Shen, P. Hauke, C. Maier, T. Brydges, C. Hempel, B. P. Lanyon, M. Heyl, R. Blatt, and C. F. Roos, Direct Observation of Dynamical Quantum Phase Transitions in an Interacting Many-Body System, Phys. Rev. Lett. **119**, 080501 (2017).

[9] W. H. Zurek, U. Dorner, and P. Zoller, Dynamics of a Quantum Phase Transition, Phys. Rev. Lett. **95**, 105701 (2005).

[10] J. Dziarmaga, Dynamics of a Quantum Phase Transition: Exact Solution of the Quantum Ising Model, Phys. Rev. Lett. **95**, 245701 (2005).

[11] B. Damski and W. H. Zurek, Dynamics of a Quantum Phase Transition in a Ferromagnetic Bose-Einstein Condensate, Phys. Rev. Lett. **99**, 130402 (2007).

[12] M. Greiner, O. Mandel, T. Esslinger, T. W. Hänsch, and I. Bloch, Quantum phase transition from a superfluid to a Mott insulator in a gas of ultracold atoms, Nature (London) **415**, 39 (2002).

[13] P. Zanardi and N. Paunković, Ground state overlap and quantum phase transitions, Phys. Rev. E **74**, 031123 (2006).

[14] S.-C. Li and L.-B. Fu, Quantum phase transition from mixed atom-molecule phase to pure molecule phase: Characteristic scaling laws and Berry-curvature signature, Phys. Rev. A **84**, 023605 (2011).

[15] P. Cejnar, P. Stránský, M. Macek, and M. Kloc, Excited-state quantum phase transitions, J. Phys. A: Math. Theor. **54**, 133001 (2021).

[16] M. A. Caprio, P. Cejnar, F. Iachello, Excited state quantum phase transitions in many-body systems, Ann. Phys. **323**, 1106 (2008).

[17] Y. Bronstein, P. Depondt, F. Finocchi, and A. M. Saitta, Quantum-driven phase transition in ice described via an efficient Langevin approach, Phys. Rev. B **89**, 214101 (2014).

[18] W.-L. You and G.-S. Tian, Quantum phase transition in the one-dimensional compass model using the pseudospin approach, Phys. Rev. B **78**, 184406 (2008).

[19] Y.-Y. Zhang, Q.-H. Chen, and K.-L. Wang, Quantum phase transition in the sub-Ohmic spin-boson model: An extended coherent-state approach, Phys. Rev. B **81**, 121105(R) (2010).

[20] Z.-C. Gu, M. Levin, and X.-G. Wen, Tensor-entanglement renormalization group approach as a unified method for symmetry breaking and topological phase transitions, Phys. Rev. B **78**, 205116 (2008).

[21] R. Wang, B. Wang, and T. A. Sedrakyan, Chern-Simons fermionization approach to two-dimensional quantum magnets: Implications for antiferromagnetic magnons and unconventional quantum phase transitions, Phys. Rev. B **98**, 064402 (2018).

[22] S. Ajisaka, F. Barra, and B. Žunkovič, Nonequilibrium quantum phase transitions in the XY model: Comparison of unitary time evolution and reduced density operator approaches, New J. Phys. **16**, 033028 (2014).

[23] S.-C. Li, L.-B. Fu, and F.-L. Li, Quantum phase transition in a three-level atom-molecule system, Phys. Rev. A **88**, 013602 (2013).

[24] H.-Q. Zhou and J. P. Barjaktarevič, Fidelity and quantum phase transitions, J. Phys. A: Math. Theor. **41**, 412001 (2008).

[25] Ö. Legeza and J. Sólyom, Two-Site Entropy and Quantum Phase Transitions in Low-Dimensional Models, Phys. Rev. Lett. **96**, 116401 (2006).

[26] Y. Qin and S.-C. Li, Quantum phase transition of a modified spin-boson model, J. Phys. A: Math. Theor. **55**, 145301 (2022).

[27] T.-L. Wang, L.-N. Wu, W. Yang, G.-R. Jin, N. Lambert, and F. Nori, Quantum Fisher information as a signature of the superradiant quantum phase transition, New J. Phys. **16**, 063039 (2014).

[28] A. Hamma, W. Zhang, S. Haas, and D. A. Lidar, Entanglement, fidelity, and topological entropy in a quantum phase transition to topological order, Phys. Rev. B **77**, 155111 (2008).

[29] R. Dillenschneider, Quantum discord and quantum phase transition in spin chains, Phys. Rev. B **78**, 224413 (2008).

[30] S.-C. Li, L. Pezzè, and A. Smerzi, Multiparticle entanglement dynamics of quantum chaos in a Bose-Einstein condensate, Phys. Rev. A **103**, 052417 (2021).

[31] F. Dimer, B. Estienne, A. S. Parkins, and H. J. Carmichael, Proposed realization of the Dicke-model quantum phase transition in an optical cavity QED system, Phys. Rev. A **75**, 013804 (2007).

[32] E. M. Bookjans, A. Vinit, and C. Raman, Quantum Phase Transition in an Antiferromagnetic Spinor Bose-Einstein Condensate, Phys. Rev. Lett. **107**, 195306 (2011).

[33] F. Iachello and N. V. Zamfir, Quantum Phase Transitions in Mesoscopic Systems, Phys. Rev. Lett. **92**, 212501 (2004).

[34] P.-B. He, Q. Sun, P. Li, S.-Q. Shen, and W. M. Liu, Magnetic quantum phase transition of cold atoms in an optical lattice, Phys. Rev. A **76**, 043618 (2007).

[35] W. Yu, J. S. Higgins, P. Bach, and R. L. Greene, Transport evidence of a magnetic quantum phase transition in electron-doped

high-temperature superconductors, Phys. Rev. B **76**, 020503(R) (2007).
[36] G.-Q. Zhang, Z. Chen, W. Xiong, C.-H. Lam, and J. Q. You, Parity-symmetry-breaking quantum phase transition via parametric drive in a cavity magnonic system, Phys. Rev. B **104**, 064423 (2021).
[37] M. Elyasi, Y. M. Blanter, and G. E. W. Bauer, Resources of nonlinear cavity magnonics for quantum information, Phys. Rev. B **101**, 054402 (2020).
[38] C. Dai, K. Xie, Z. Pan, and F. Ma, Strong coupling between magnons confined in a single magnonic cavity, J. Appl. Phys. **127**, 203902 (2020).
[39] G. Flower, M. Goryachev, J. Bourhill, and M. E. Tobar, Experimental implementations of cavity-magnon systems: from ultra strong coupling to applications in precision measurement, New J. Phys. **21**, 095004 (2019).
[40] B. Wang, C. Kong, Z.-X. Liu, H. Xiong, and Y. Wu, Magnetic-field-controlled magnon chaos in an active cavity-magnon system, Laser Phys. Lett. **16**, 045208 (2019).
[41] R.-C. Shen, Y.-P. Wang, J. Li, S.-Y. Zhu, G. S. Agarwal, and J. Q. You, Long-Time Memory and Ternary Logic Gate Using a Multistable Cavity Magnonic System, Phys. Rev. Lett. **127**, 183202 (2021).
[42] Q. Cai, J. Liao, B. Shen, G. Guo, and Q. Zhou, Microwave quantum illumination via cavity magnonics, Phys. Rev. A **103**, 052419 (2021).
[43] Y.-P. Wang, G.-Q. Zhang, D. Zhang, X.-Q. Luo, W. Xiong, S.-P. Wang, T.-F. Li, C.-M. Hu, and J. Q. You, Magnon Kerr effect in a strongly coupled cavity-magnon system, Phys. Rev. B **94**, 224410 (2016).
[44] G. Zhang, Y. Wang, and J. You, Theory of the magnon Kerr effect in cavity magnonics, Sci. China Phys. Mech. Astron. **62**, 987511 (2019).
[45] C. Zhao, R. Peng, Z. Yang, S. Chao, C. Li, Z. Wang, and L. Zhou, Nonreciprocal amplification in a cavity magnonics system, Phys. Rev. A **105**, 023709 (2022).
[46] Y. Wang, W. Xiong, Z. Xu, G.-Q. Zhang, and J.-Q. You, Dissipation-induced nonreciprocal magnon blockade in a magnon-based hybrid system, Sci. China Phys. Mech. Astron. **65**, 260314 (2022).
[47] C. Zhang, C. Jia, Y. Shi, C. Jiang, D. Xue, C. K. Ong, and G. Chai, Nonreciprocal multimode and indirect couplings in cavity magnonics, Phys. Rev. B **103**, 184427 (2021).
[48] Y. T. Zhao, J. W. Rao, Y. S. Gui, Y. P. Wang, and C.-M. Hu, Broadband Nonreciprocity Realized by Locally Controlling the Magnon's Radiation, Phys. Rev. Applied **14**, 014035 (2020).
[49] M. X. Bi, X. H. Yan, Y. Zhang, and Y. Xiao, Tristability of cavity magnon polaritons, Phys. Rev. B **103**, 104411 (2021).
[50] W. Yu, T. Yu, and G. E. W. Bauer, Circulating cavity magnon polaritons, Phys. Rev. B **102**, 064416 (2020).
[51] Y.-P. Wang, G.-Q. Zhang, D. Zhang, T.-F. Li, C.-M. Hu, and J. Q. You, Bistability of Cavity Magnon Polaritons, Phys. Rev. Lett. **120**, 057202 (2018).
[52] B. Wang, Z.-X. Liu, C. Kong, H. Xiong, and Y. Wu, Magnon-induced transparency and amplification in $\mathcal{PT}$-symmetric cavity-magnon system, Opt. Express **26**, 20248 (2018).
[53] D. Xie, C. Xu, and A. M. Wang, Parameter estimation and quantum entanglement in PT symmetrical cavity magnonics system, Results Phys. **26**, 104430 (2021).
[54] Y. Yang, Y.-P. Wang, J. W. Rao, Y. S. Gui, B. M. Yao, W. Lu, and C.-M. Hu, Unconventional Singularity in Anti-Parity-Time Symmetric Cavity Magnonics, Phys. Rev. Lett. **125**, 147202 (2020).
[55] J. Zhao, Y. Liu, L. Wu, C.-K. Duan, Y.-X. Liu, and J. Du, Observation of Anti-$\mathcal{PT}$-Symmetry Phase Transition in the Magnon-Cavity-Magnon Coupled System, Phys. Rev. Applied **13**, 014053 (2020).
[56] D. F. Walls and G. J. Milburn, *Quantum Optics* (Springer, Berlin, 2007).
[57] C. W. Gardiner and M. J. Collett, Input and output in damped quantum systems: Quantum stochastic differential equations and the master equation, Phys. Rev. A **31**, 3761 (1985).
[58] C. W. Gardiner and P. Zoller, *Quantum Noise* (Springer, Berlin, 2000).
[59] C. Emary and T. Brandes, Chaos and the quantum phase transition in the Dicke model, Phys. Rev. E **67**, 066203 (2003).
[60] I. S. Gradshteyn and I. M. Ryzhik, *Table of Integrals, Series and Products* (Academic, Orlando, 1980).
[61] X. H. H. Zhang and H. U. Baranger, Driven-dissipative phase transition in a Kerr oscillator: From semiclassical $\mathcal{PT}$ symmetry to quantum fluctuations, Phys. Rev. A **103**, 033711 (2021).
[62] R. G. E. Morris, A. F. van Loo, S. Kosen, and A. D. Karenowska, Strong coupling of magnons in a YIG sphere to photons in a planar superconducting resonator in the quantum limit, Sci. Rep. **7**, 11511 (2017).
[63] P. Krantz, A. Bengtsson, M. Simoen, S. Gustavsson, V. Shumeiko, W. D. Oliver, C. M. Wilson, P. Delsing, and J. Bylander, Single-shot read-out of a superconducting qubit using a Josephson parametric oscillator, Nat. Commun. **7**, 11417 (2016).
[64] S. Blundell, *Magnetism in Condensed Matter* (Oxford University Press, Oxford, 2001).
[65] D. D. Stancil and A. Prabhakar, *Spin Waves* (Springer, Berlin, 2009).
[66] J. R. Macdonald, Ferromagnetic Resonance and the Internal Field in Ferromagnetic Materials, Proc. Phys. Soc. A **64**, 968 (1951).
[67] Ö. O. Soykal and M. E. Flatté, Strong Field Interactions between a Nanomagnet and a Photonic Cavity, Phys. Rev. Lett. **104**, 077202 (2010).
[68] T. Holstein and H. Primakoff, Field Dependence of the Intrinsic Domain Magnetization of a Ferromagnet, Phys. Rev. **58**, 1098 (1940).